Acta Materialia 282 (2025) 120468

Contents lists available at ScienceDirect

Acta Materialia

journal homepage: www.elsevier.com/locate/actamat

Ab initio investigation of ZnV_2O_4, ZnV_2S_4, and ZnV_2Se_4 as cathode materials for aqueous zinc-ion batteries

O.M. Sousa [a,*], F. Sorgenfrei [b], F.O. Carvalho [c], L.V.C. Assali [d], M.V. Lalic [c], P. Thunström [b], C.Moyses Araujo [b,e,f,*], O. Eriksson [b,g], H.M. Petrilli [d], A.B. Klautau [a]

[a] Universidade Federal do Pará, Faculdade de Física 66075110, Belém, PA, Brazil
[b] Uppsala University, Department of Physics and Astronomy, Box 516 SE-75120, Uppsala, Sweden
[c] Universidade Federal de Sergipe, Departamento de Física 49100-000, São Cristóvão, SE, Brazil
[d] Universidade de São Paulo, Instituto de Física, Rua do Matão, 1371 05508-090, São Paulo, SP, Brazil
[e] Karlstad University, Department of Engineering and Physics 65188 Karlstad, Sweden
[f] Wallenberg Initiative Materials Science for Sustainability (WISE), Karlstad University, Department of Engineering and Physics 65188 Karlstad, Sweden
[g] Wallenberg Initiative Materials Science for Sustainability (WISE), Uppsala University, Box 516 SE-75120, Uppsala, Sweden

ARTICLE INFO

Keywords:
Cathode materials
ZnV_2O_4
ZnV_2S_4
ZnV_2Se_4
density functional theory
Zinc-ion batteries

ABSTRACT

Zinc-ion batteries (ZIBs) employing aqueous electrolytes have emerged as one of the most promising alternatives to lithium-ion batteries (LIBs). Nonetheless, the development of ZIBs is hindered by the scarcity of cathode materials with suitable electrochemical properties. In this work, we investigate the unique properties of zinc vanadate oxide (ZnV_2O_4, ZVO) and zinc vanadate sulfide (ZnV_2S_4, ZVS) compounds as cathode materials, focusing on their crystal structures, electrochemical performance, spectroscopic features and potential applications in ZIBs. Additionally, we investigate a new cathode material, zinc vanadate selenide (ZnV_2Se_4, ZVSe), constructed by replacing sulfur with selenium in the ZVS cubic structure. Our findings reveal that these compounds exhibit distinct electronic and electrochemical properties, although they have similar magnetic properties due to the fact that vanadium has the same oxidation state in all three compounds. On average, ZVS stands out as the most promising candidate for ZIBs cathodes, followed by ZVO. ZVSe, shows lower electrochemical performance and also has the obvious drawback of being more costly than the sulfur- and oxygen-based compounds. Our theoretical results align closely with available experimental data, both for electrochemical properties as well as x-ray and photoelectron spectroscopy, where a comparison can be made.

1. Introduction

Lithium-ion batteries (LIBs) are extensively used in a variety of applications, such as electric vehicles, mobile phones, and laptops, owing to their high energy storage capacity, long life cycle, and portability. However, the rapid increase in electric vehicle production is expected to lead to a gradual shortage of metallic lithium resources, raising concerns about its impact on sustainable development [1]. Alternative types of ion batteries, including sodium [2,3], potassium [4,5], magnesium [6,7], calcium [8,9], zinc [10,11] or aluminum [12,13] are now being explored.

Zinc-ion batteries (ZIBs), employing aqueous electrolytes, have emerged as promising alternatives to LIBs [14–20] due to their similar ionic radii, abundance in the Earth's crust, high volumetric energy density, low cost, environmental compatibility, large redox potential against the standard hydrogen electrode (SHE), and stability of metallic zinc (see Table S1 of the Supplementary Information (SI) for zinc and lithium characteristics). The two-electron transfer mechanism of Zn can lead to a high volumetric energy density during the cycling process [21].

Despite these advantages, the lack of suitable cathode materials for the battery charge/discharge process is the main factor hindering the advancement of ZIBs. As a result, several cathode materials are being produced and tested to overcome this limitation, but the cathode materials reported so far for ZIBs with aqueous electrolytes face significant challenges. For example, Mn-based oxides suffer a marked reduction in their capacity due to irreversible structural changes caused by the dissolution of Mn in the electrolyte [22,23]; similarly, Prussian blue analogs, despite maintaining a considerable battery life cycle, exhibit

* Corresponding authors.
E-mail addresses: osmarufpa@gmail.com (O.M. Sousa), Moyses.Araujo@kau.se (C. Araujo).

https://doi.org/10.1016/j.actamat.2024.120468
Received 9 August 2024; Received in revised form 7 October 2024; Accepted 9 October 2024
Available online 10 October 2024

very low specific capacity [24,25].

Spinel-type (AB_2Y_4) materials have good applications in batteries. Among them, vanadium-based compounds became an important research topic in the development of cathodes for use in ZIBs [26,27], due to their multiple oxidation states (+II, +III, +IV, and +V), low cost, and environmental compatibility [28–34]. Recently, the electrochemical properties of ZnV_2S_4 (ZVS) [30] pointed to a great potential to be used as a cathode material in ZIBs. With a structure analogous to ZnV_2S_4, ZnV_2O_4 (ZVO) also emerged as a promising candidate for a cathode material to be used in ZIBs [31]. ZVO and ZVS electrochemical performances, in aqueous electrolytes, as well as for some other cathode materials available in the literature, are summarized in Table S2 of the SI, where it can be noticed that ZVS presents excellent cycling performance compared to other cathode materials, while ZVO exhibits only reasonable performance. It is important to highlight that although ZVO has a relatively low-capacity retention rate compared to other current cathodes, its other electrochemical properties (structural stability, electrical and ionic conductivities, among others) are worth investigating, since it has been experimentally proven that there are techniques to solve the retention problem as in, for example, the $ZnMn_2O_4$ case [35-39].

In addition to ZVO and ZVS, which have already been synthesized experimentally, here we also investigate ZnV_2Se_4 (ZVSe), a new possible cathode material, by replacing sulfur with selenium in the stoichiometric cubic structure of ZVS. Cycling performance properties can only partially characterize a compound as a promising cathode material for use in ZIBs. Our goal here is, by using a theoretical approach in the framework of the Density Functional Theory (DFT), to inspect and describe several distinctive properties of ZVS, ZVO, and ZVSe cathode materials through the examination of their crystal structures, structural and electronic behavior during zinc extraction, electrochemical performance as well as potential applications in ZIBs. This study also has the ambition to shine light on spectroscopic features of these materials, since both x-ray- and photoelectron spectroscopy are frequently used as characterization tools for their physical and chemical properties.

It is worth noting that the cubic phases of ZVO [40,41], ZVS [42] and ZVSe [43] compounds without Zn deficiency have already been theoretically investigated by calculations based on first-principle, density functional theory. However, the complete mapping of the properties of these materials during Zn extraction and their potential for application in ZIBs are here described for the first time. An in-depth understanding of these materials is crucial in driving the development of more efficient, cost-effective, and sustainable energy storage technologies.

2. Methodology and calculation details

The first-principles calculations were carried out using the all-electron spin-polarized full-potential linearized augmented plane wave (FP-LAPW) method [44], implemented in the WIEN2k computational package [45], within the framework of the DFT [46,47]. The cut-off at $K_{max} = 7.0/R_{MT}$ was employed to limit the number of plane-waves in the interstitial region. The atomic muffin-tin radii (R_{MT}) were chosen to be R_{MT}(V) = 1.80, R_{MT}(Zn) = 1.95, and R_{MT}(O, S and Se) = 1.60 atomic units (a.u.). The electronic valence configurations used were Zn: $3p^6 3d^{10} 4s^2$, V: $3s^2 3p^6 3d^3 4s^2$, O: $2s^2 2p^4$, S: $3s^2 3p^4$ and Se: $3d^{10} 4s^2 4p^4$. The Brillouin zone integration has been performed upon the 3 × 3 × 3 k-point grid (14 k-points in the irreducible zone), according to the Monkhorst-Pack scheme [48].

The exchange-correlation effects were described by the generalized gradient approximation (GGA), within Perdew-Burke-Ernzerhof parametrization (PBE) [49] combined with the Hubbard-U potential [50–53] to describe the electronic correlation among the V-3d electrons in a mean-field approximation. We calculated the U values in a self-consistent manner [52,53], and the corresponding values are presented in Table S3 of the SI. In the literature, only the ZVO experimental band gap value is available. The band gap width obtained for ZVO with the calculated U value was 1.80 eV, which underestimates the experimental value of 2.80–2.95 eV [54,55]. We performed tests to determine the U value that would align the theoretical band gap with the experimental one. We found that a U value of 6.5 eV yielded a theoretical band gap of 2.70 eV, significantly closer to the experimental value than the band gap obtained using the self-consistently calculated U value. The semi-local modified Becke-Johnson (mBJ) potential offers an alternative approach to accurately determine the band gap width [56]. This potential has demonstrated enhanced accuracy in describing band gap widths for diverse semiconductors and insulators, as evidenced by numerous studies [57–63]. The band gap width of ZVO, calculated using the spin-polarized mBJ approach, was 2.92 eV, closely matching the experimental value. The ZVS and ZVSe band gap values, also obtained using this approach, were 0.6 eV and 0.30 eV, respectively. The band gaps calculated using the mBJ potential for the ZVS and ZVSe materials are consistent with those obtained by the GGA + U method, where the U values were determined in a self-consistent manner (Table S3). In this work, the mBJ potential was solely employed for band gap and electronic structure calculations, while the GGA + U method, with the U value calculated in a self-consistent manner, was used for all other property calculations such as lattice parameter, average voltage, energy density, energy barrier and contraction volume.

The calculations were carried out in both ferromagnetic (FM) and antiferromagnetic (AFM) ordering. Our findings revealed that at $T = 0$ K, the AFM alignment for the ZVO, ZVS and ZVSe compounds exhibited a total energy, per formula unit, of 10.6×10^{-2} eV/f.u., 1.1×10^{-2} eV/f.u. and 1.6×10^{-2} eV/f.u. lower than that of the FM alignment, respectively. We conducted some tests performing calculations with both FM and AFM alignments and found that the only significant change (when making FM or AFM calculations) in the cathodic properties of these materials is in the band gap width and consequently in their electronic structures. The theoretical specific capacity, average voltage, energy density, volume contraction/expansion, and ionic conductivity practically do not change concerning the magnetic ordering. For example, the average voltage and energy density results for the ZVS with AFM ordering are 1.13 V and 204.95 Wh/kg, respectively, and with FM ordering, are 1.12 V and 203.14 Wh/kg, respectively. However, the band gap width is fundamental in the simulations of cathode materials, as it directly influences the electrical conductivity; therefore, in contrast to previous works [40–43], all calculations in the present investigation were performed using AFM ordering. Our calculations were carried out considering the compound's conventional cells with 56 atoms ($Zn_8V_{16}Y_{32}$, with $Y = O, S, Se$).

The average open circuit voltage was calculated based on the following formula:

$$V = \frac{-[E(Zn_x\ V_2Y_4) - E(V_2Y_4) - xE(Zn)]}{nx}, \quad (1)$$

where $E(Zn_xV_2Y_4)$ are the compounds DFT total energies, while $E(V_2Y_4)$ are the total energies when all Zn ion of the ZVO, ZVS and ZVSe were extracted; $E(Zn)$ are the energy of the Zn standard ground state, i.e., the DFT total energy of metallic hcp Zn, per atom, and n is the number of transferred electrons, per Zn atom. The theoretical specific capacity of the ZVO, ZVS, and ZVSe can be calculated by

$$Q = \frac{nF}{3.6\ m}, \quad (2)$$

where F is the Faraday constant and m is the electrode molar mass.

Ionic diffusion was calculated with the Cambridge Sequential Total Energy Package (CASTEP) plane-wave code [64], using on-the-fly generated (OTFG) ultrasoft pseudopotentials [65]. The exchange-correlation effects were described by the GGA-PBE functional [49] and a cutoff energy of 550 eV was considered for the plane wave basis set. The irreducible part of the Brillouin zone was sampled by a 14

K-points mesh, following the Monkhorst-Pack scheme [48]. The atomic valence electron configurations were Zn: $3p^6 3d^{10} 4s^2$, V: $3s^2 3p^6 3d^3 4s^2$, O: $2s^2 2p^4$, S: $3s^2 3p^4$ and Se: $3d^{10} 4s^2 4p^4$. The CASTEP computational code does not have the mBJ exchange-correlation potential implemented; therefore, the ionic diffusion calculations were performed using only the GGA + U approach. The U values for the V 3d-states were 6.5 eV (ZVO), 3.63 eV (ZVS), and 3.49 eV (ZVSe). The band gap widths of 2.78 eV for ZVO, 0.69 eV for ZVS, and 0.25 eV for ZVSe, using these U values, agree with those obtained by the mBJ approach used in WIEN2k simulations. This indicates that the diffusion energy barriers, which were obtained by applying a full linear and quadratic synchronous transit (LST/QST) transition state (TS) search algorithm in CASTEP [66], are well described.

We also investigated the V $L_{2,3}$-edge X-ray photoelectron spectroscopy (XPS) and $L_{2,3}$-edge XANES. To do this we solved the DFT problem using the code RSPt [67,68], based on linear muffin-tin orbitals (LMTO) and a full-potential geometry, and used Löwdin orthogonalized LMTO's, denoted as "ORT' in Refs. [69,70], for the correlated orbitals that were defined in an energy window of [−10.2, 6.8] eV. With these orbitals a multiconfiguration approach was used to calculate the XPS and XANES spectra, in the dipole approximation. The exact procedure to calculate the XANES is outlined in Refs. [71,72], and the software used in these calculations can be downloaded from Ref. [73]. A few salient features of the calculation should be noted; the local Hamiltonian in the ORT basis was allowed to hybridize with 3 bath states per correlated orbital, to describe the interaction with the rest of the lattice. A representation of the fit of the hybridization function of the e_g and t_{2g} orbitals of ZnV_2O_4 can be observed in Figure S1 of the SI. The higher-order Slater parameters were calculated using the Slater integrals that were scaled to 80% of their calculated values, due to screening effects not included in the expression of the Slater integrals. Also, we used our estimate of 6.5 eV and 3.63 eV of the Hubbard U for the zeroth order parameter ${F_{dd}}^0$ for ZVO and ZVS, respectively. The zeroth order parameter ${F_{pd}}^0$ has been estimated as ${F_{pd}}^0 = 1.3\,{F_{dd}}^0$. As a final comment on this section, note that the XPS was calculated in the same manner as the XANES spectrum, with the only difference being that the transition operator in the XPS does not excite the 2p-electrons into the empty 3d-orbitals but instead excite them into a decoupled unbound state.

3. Results and discussion

3.1. ZVO, ZVS and ZVSe without Zn deficiency

Under ambient conditions, ZVO and ZVS crystallize in a cubic structure with the space group $Fd\bar{3}m$ (#227). V^{3+} ions occupy octahedral sites (Wyckoff atomic position 16c), while Zn^{2+} ions are located in tetrahedral sites (8b), as shown in Figure S2 of the SI. After replacing S by Se in the ZVS structure, the resulting ZVSe structure remains belonging to the $Fd\bar{3}m$ group.

Firstly, the lattice parameters of ZVO, ZVS, and ZVSe were optimized, and their atomic positions were relaxed. In the subsequent step, we obtained the electronic structure of the materials. Table 1 shows the results of the lattice parameters, band gap widths, vanadium oxidation states and magnetic moments for the stoichiometric configurations. The lattice parameters are in excellent agreement with the available experimental data. The V^{3+} ion has 2 unpaired 3d electrons; therefore, it is expected that the magnetic moment must be around 2 μ_B, as obtained by our calculations. Compared with the experimental value, it can be observed that the ZVO band gap is well described using the mBJ approach. To the best of our knowledge, no experimental results regarding the ZVS and ZVSe band gap widths have been yet reported. As shown in Table 1, the ZVSe compound has the narrowest band gap, therefore it is the one that exhibits the best electronic conductivity among the three of them. Similarly, the ZVS compound presents better electronic conductivity compared to ZVO.

Table 1
Theoretical lattice parameters, vanadium spin magnetic moments (μ), and the direct transition band gap widths of ZVO, ZVS, and ZVSe compounds, with available experimental data. Here "a" represents the results obtained with the U value adjusted to the experimental band gap, and "m" represents the results obtained with the mBJ potential.

	a(Å)	$\mu(\mu_B)$	band gap (eV)
Theor.			
ZnV_2O_4	8.47	$1.60^{a}/1.64^{m}$	$2.70^{a}/2.92^{m}$
ZnV_2S_4	10.10	1.64^{m}	0.60^{m}
ZnV_2Se_4	10.34	1.66^{m}	0.30^{m}
Expt.			
ZnV_2O_4	8.40[74]	—	2.80[54]/2.95[55]
ZnV_2S_4	10.07[30]	—	—

The ZVO, ZVS, and ZVSe partial densities of states (PDOS) calculated with mBJ potential are shown in Fig. 1. Without zinc deficiency, all compounds contain only a type of vanadium ion oxidation state in their structure (V^{3+}). The crystals split the V^{3+} 3d-related states and the electronic configuration is given by t_{2g}^2 and e_g^0. The top of the valence band and the bottom of the conduction band of ZVO, ZVS, and ZVSe are dominated by the V-related 3d-orbitals.

3.2. ZVO, ZVS, and ZVSe with Zn deficiency

The modifications in the properties of ZVO, ZVS, and ZVSe with zinc extraction were investigated by constructing various structures with several zinc concentrations [$Zn_xV_2Y_4$, $0 \le x \le 1$, and $Y = O, S, Se$]. Subsequently, the crystal structures, electrochemical performances, and potential applications in zinc batteries were analyzed. All the properties that characterize the ZVO, ZVS, and ZVSe as potential cathode materials for use in ZIBs are shown in Table 2. As can be observed, ZVO exhibited the highest theoretical specific capacity, the highest energy density, and the lowest diffusion energy barrier, properties that characterize it as a suitable cathode material. However, it also displayed the lowest electronic conductivity and the highest volume contraction when all zinc ions are removed. This ZVO volume contraction of 12.3%, although not ideal, falls within acceptable values for cathodes used in zinc batteries [75]. The host matrix is expected to undergo a more significant change in volume during the insertion/extraction of divalent ions compared to monovalent, as shown in our previous work [76]. The electronic conductivity, in turn, can be improved, for example, by doping and co-doping. Therefore, under certain conditions, ZVO has potential as a cathode material to be used in ZIBs.

The ZVSe compound exhibited only a small volume contraction when all zinc ions were removed, an excellent characteristic for battery applications. Furthermore, it presented a narrow band gap width, indicating good electric conductivity. However, the ZVSe presented low specific capacity, low voltage, low energy density, and a high diffusion energy barrier compared to ZVO and ZVS, properties that hinder its application as a cathode material to be used in ZIBs. It is worth noting that this compound is a theoretical prediction, since it has not yet been synthesized. Although ZVSe does not exhibit favorable electrochemical performance, it can be used for other applications that require materials with narrow band gaps and that undergo small changes in their structures. Therefore, the ZVSe properties investigated in this work can be very useful for providing new insights to applications that require small band gaps.

The ZVS was the compound that presented the best properties on average and is positioned as a promising candidate to be used as a cathode in zinc batteries. The theoretical specific capacity is higher than other commercialized cathodes, such as $LiMn_2O_4$ (capacity = 148 mAh/g) and $LiFePO_4$ (capacity = 170 mAh/g) [77]. The energy barrier (eb) is lower than that of other spinel-type materials that were predicted by machine learning as potential cathodes for use in zinc batteries, such as

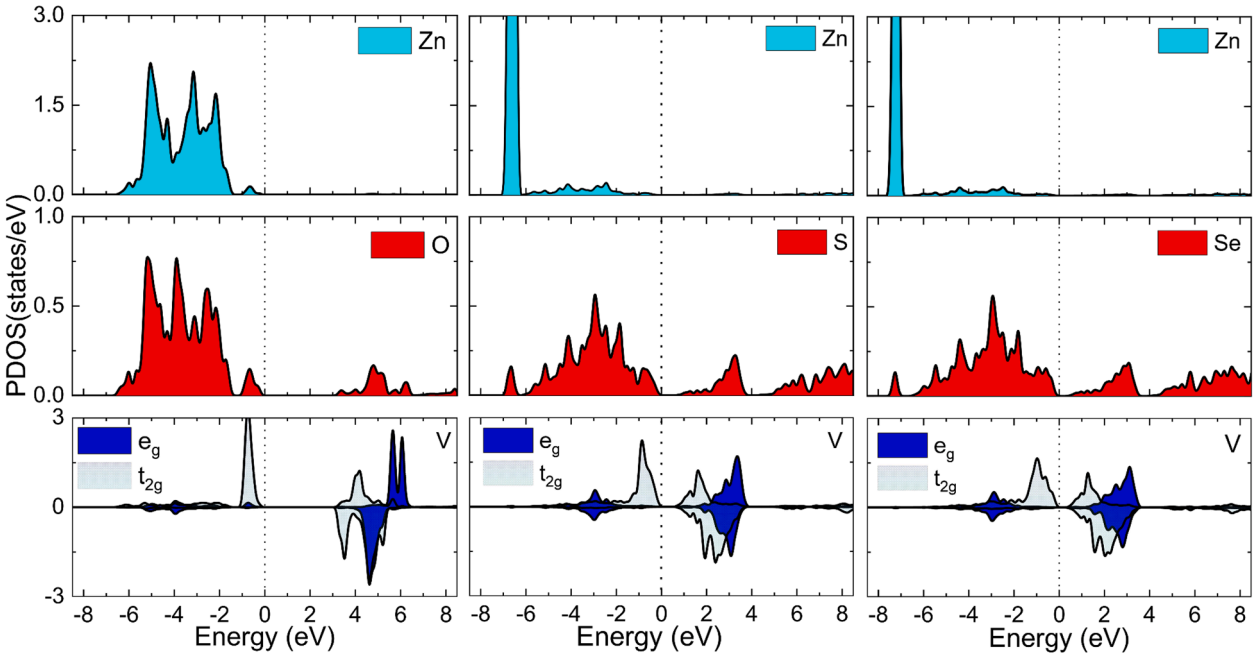

Fig. 1. Partial density of states (PDOS) calculated with WIEN2k code and using the mBJ potential of ZVO, ZVS, and ZVSe. The dashed lines represent the top of the valence band, i.e., the highest occupied energy level (Fermi energy).

Table 2
Theoretical specific capacity (mAh/g), average voltage (V), energy density (Wh/kg), energy barrier (eV), contraction volume (CV in %), and band gap width (eV) of ZVO, ZVS, and ZVSe compounds, along with experimental data. "c" represents the results obtained with the calculated self-consistently U value, "a" represents the results obtained with the U value adjusted to the experimental band gap, and "m" represents the results obtained with the mBJ potential.

Cathode	Capacity	Voltage	Energy density	Energy Barrier	CV	Band Gap
Theor.						
ZnV_2O_4	231.78	1.02^c/ 1.35^a	236.41^c/ 312.9^a	0.16^c/ 0.19^a	12.3^c	1.80^c/ 2.70^a/ 2.9^m
ZnV_2S_4	181.38	1.13^c	204.95^c	0.24^c	7.6^c	0.72^c/ 0.60^m
ZnV_2Se_4	110.95	0.51^c	56.58^c	0.68^c	3.7^c	0.22^c/ 0.30^m
Expt.						
ZnV_2O_4	—	$\approx$ 0.8[31]	—	—	—	2.80[54] /2.95[55]
ZnV_2S_4	—	$\approx$ 1.0[30]	—	—	—	—

$ZnSn_2S_4$ (eb = 0.95 eV), $ZnMo_2S_4$ (eb = 0.70 eV), $ZnMn_2S_4$ (eb = 0.43 eV), $ZnFe_2S_4$ (eb = 0.77 eV), $ZnCu_2S_4$ (eb = 0.77 eV), $ZnCa_2S_4$ (eb = 0.29 eV), and $MgZn_2S_4$ (eb = 0.42 eV) [75]. It is worth noting that in this theoretical prediction, the authors found an energy barrier of only 0.0019 eV for $ZnNi_2O_4$ and 0.09 eV for $ZnCu_2O_4$; however, these compounds experienced volume variations of 20.10% and 17.95%, respectively [75].

In contrast to the theoretical predictions obtained from machine learning, ZVS and ZVO have already been experimentally synthesized as cathodes; therefore, our results have good validation, since we were able to reproduce experimental results, which strengthens our theoretical predictions. The calculated voltage for ZVO and ZVS agree reasonably well with experimental results. The complete behavior of the lattice parameters and volume of ZVO, ZVS, and ZVSe as a function of zinc concentration are presented in Figure S3 and Table S4 of the SI, while Figures S4 and S5 illustrate the diffusion pathways of Zn^{2+} ions and the corresponding energy barriers within the ZVO, ZVS, and ZVSe structures. As pointed out earlier, the ZVSe does not have potential to be used as a cathode material in ZIBs and, consequently, an analysis described below will be carried out only for the ZVO and ZVS compounds.

As demonstrated in our previous work [76], X-ray absorption near-edge structure (XANES) is a powerful technique for mapping the redox process in battery materials. In this work, we used the WIEN2k code plus mBJ potential to calculate the vanadium K-edge XANES spectrum of ZVO and ZVS compounds. By analyzing this edge, it is possible to characterize the vanadium oxidation/reduction during battery charge/discharge. The core-hole effect was considered, meaning one electron was removed from the vanadium ion 1*s* orbital and placed at the bottom of the conduction band, which approximately corresponds to the final state of the X-ray absorption process. Full details of how these calculations are performed can be found in a previous work, where we successfully evidenced the manganese oxidation process in the $ZnMn_2O_4$ and $LiMn_2O_4$ compounds during battery charging [76].

The ZVO and ZVS theoretical XANES spectra, calculated for the $x = 1$ zinc concentration, are shown in Figs. 2a and 2b, respectively. The vanadium K-edge XANES spectra were generated by electric dipole-forbidden transition from the 1*s* electron to an unoccupied 3*d* orbital (pre-edge) and by dipole-allowed transitions from the vanadium 1*s* electron to the conduction empty bands above the Fermi energy. The peaks above the pre-edge region are attributed to the dipole-allowed $1s \rightarrow 4p$ transition. The theoretical vanadium K-edge XANES spectra for $Zn_xV_2S_4$ and $Zn_xV_2O_4$, calculated for $x = 1$ and $x = 0$ zinc concentrations are illustrated in Figs. 2c and 2d. The spectra for $x = 0$ shifted to higher energies during the extraction of zinc due to the increase of the V oxidation state. The absorption edge shift indicates that V^{3+} ions are being oxidized to V^{4+}. V^{4+} ions are more strongly bonded to the oxygen atoms and require more energy to be excited, which causes the shift of the absorption edge to higher energies.

Fig. 2b compares the ZVO obtained results for $x = 1$ concentration with experimental data available in the literature [78]. The experimental energy range was adjusted to the theoretical energy range (for justification see our previous work [76]). The results for the vanadium K-edge XANES spectra align well with the experimental ones for $x = 1$. All main peaks determined theoretically (a, b, c, and d) are in

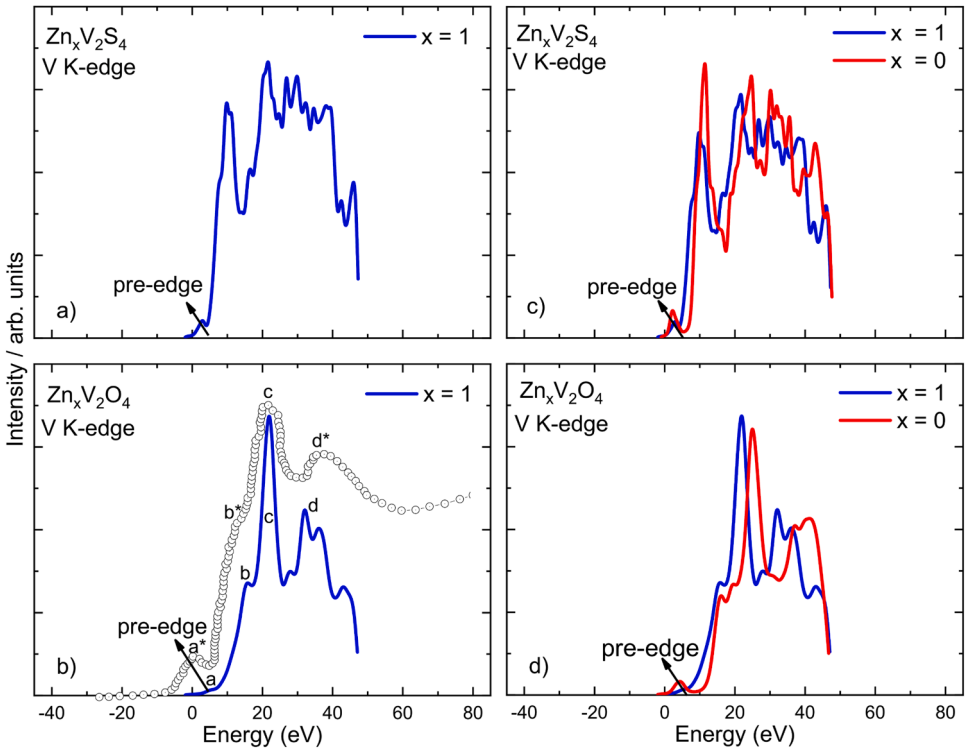

Fig. 2. Theoretical vanadium K-edge XANES spectra for $x = 1$ for a) ZVS and b) ZVO, compared to experimental results [78]. Calculated vanadium K-edge XANES spectra at $x = 1$ and $x = 0$ zinc concentrations for c) ZVS and d) ZVO. Calculations performed using the WIEN2k code with the mBJ potential.

concordance with those observed experimentally (a*, b*, c* and d*) [78]. This fact demonstrates that the electronic structures of the materials have been accurately calculated. To the best of our knowledge, no experimental results regarding the vanadium K-edge XANES spectra of ZVS have been reported.

We show the calculated V $L_{2,3}$-edge XPS for $Zn_xV_2O_4$ and $Zn_xV_2S_4$ for both $x = 1$ and $x = 0$ in Fig. 3. Note that all spectra have been shifted in energy so that their L_3-edge aligns with the experimental L_3-edge of ZVO. In Fig. 3a, we compare the experimental and calculated $L_{2,3}$-edge XPS of ZVO with $x = 1$. As shown, theory reproduces the experimental

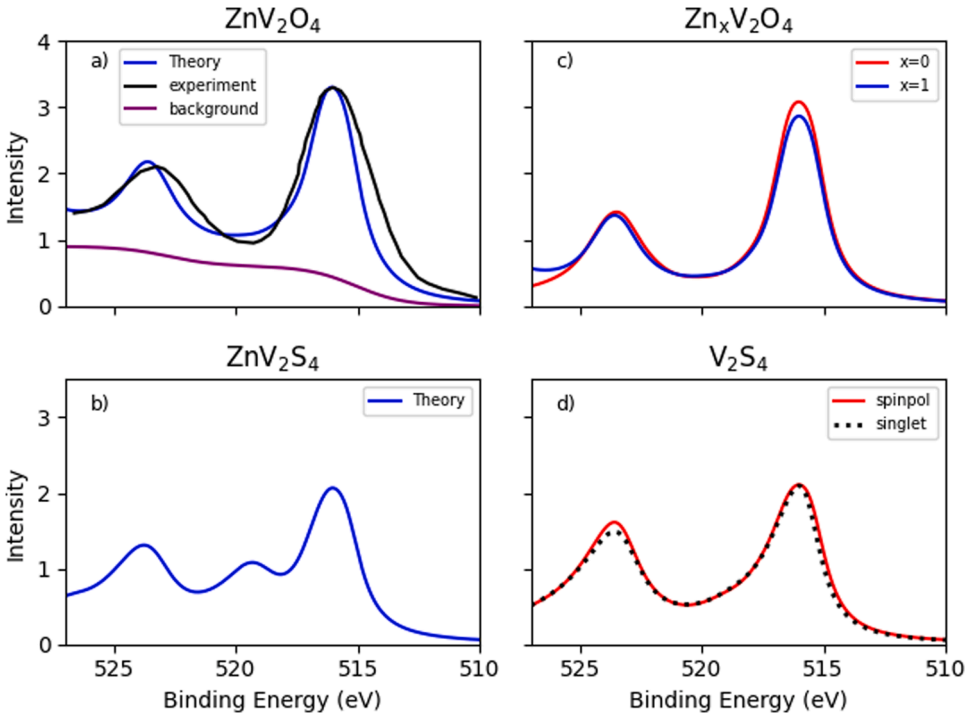

Fig. 3. Theoretical vanadium $L_{2,3}$-edge XPS spectra for $x = 1$ for a) ZVO and b) ZVS, compared to experimental results [79]. Calculated vanadium $L_{2,3}$-edge XPS spectra at $x = 1$ and $x = 0$ zinc concentrations for c) ZVO and for d) the singlet and spin polarized state of zinc removed ZVS. Calculations performed using the RSPt code.

spectra quite well. In Fig. 3b, we plot the calculated $L_{2,3}$-edge XPS of ZVS, which shows a satellite peak between the L_3 and L_2-edges. A comparison of the calculated $L_{2,3}$-edge XPS of ZVO for $x = 0$ and $x = 1$ can be seen in Fig. 3c. Here, one can observe that the spectra are very similar to one another, and the only change seems to be that both the L_3-edge and the L_2-edge becomes somewhat larger in intensity when zinc is removed from the system. In the case of the zinc removed ZVS, we found two qualitatively different competing ground state solutions with a relative energy difference of <10 meV. The first one is a spin singlet state, while the other has a local spin moment. This competition is only observed in this material, because the V 3*d* orbitals strongly hybridize with the S 2*p* at the Fermi energy. Both states are sensitive to the hybridization and therefore the local environment of the vanadium atom. We present both solutions in Fig. 3d, because both solutions or a mixture of both could be possible in a sample depending on disorder or defects in the crystal structure. The XPS of both states is similar with the spin polarized state having a higher intensity on the L_2-edge. Comparing the XPS of both states to the XPS of the ZVS with $x = 1$, we can see the same changes as in ZVO and a disappearance of the satellite peak.

In Fig. 4, the calculated V $L_{2,3}$-edge XAS for ZVO and ZVS is plotted for both $x = 1$ and $x = 0$. All spectra have been shifted so that the main peak of the L_3-edge aligns with the experimental L_3-edge of $Zn_{0.9}Li_{0.1}V_2O_4$ [80], which is the closest system for which we found experimental data. In Fig. 4a, we compare the calculated $L_{2,3}$-edge XAS for ZVO with the experimental $L_{2,3}$-edge XAS of $Zn_{0.9}Li_{0.1}V_2O_4$. It is clear that we reproduce all features that can be observed in the experiment but some of the calculated features have slightly lower intensity. In particular, the calculation reproduces the small but clearly visible satellite peak between the L_3 and the L_2-edges. In Fig. 4b, we show the calculated $L_{2,3}$-edge XAS of ZVS. Compared to ZVO one can see that the satellite peak is shifted to higher energies and that the L_2-edge only consists of a single peak. Unfortunately, no XANES experimental data is available for this system, similar to the lack of XPS data, and the theory presented here serves as a prediction. Fig. 4c shows the effect of zinc being removed from ZVO. One can see that the main peak of the L_3-edge shrinks and that all other peaks move slightly to lower energies. It should be noted that the two L_3-edge main peaks have been aligned, which means that the energy shift due to the removal of zinc is not included in the figure. In Fig. 4d, we can see the XAS of the singlet and spin polarized state of zinc removed ZVS, which both look distinct from the pristine ZVS spectra. Similar to ZVO, the left shoulders of the L_3 and L_2 edges are more pronounced after zinc removal in both states. This effect is more pronounced in ZVS compared to ZVO, and it is most prominent when transitioning to the singlet state. Note that the background that was added to Fig. 3a and Fig. 4a to compare with the experiment is comprised of two step-like functions, which are located at the maxima of the L_3 and the L_2-edge. For the step-like functions we used the Fermi-Dirac distribution as outlined in [81]. Also, the Lorentzian broadening due to lifetime effects of the L_3 and L_2-edges in XAS and XPS have been fitted to match the width of the corresponding experiment of ZVO. The same broadening parameter is then applied to all systems even if the lifetimes of the excited states could change between systems.

The total density of states (TDOS) at $x = 1$ and $x = 0$ for the ZVO and ZVS are illustrated in Figure S6 of the SI. At $x = 1$, the ZVO has a calculated band gap of 2.92 eV, and at $x = 0$ the width is 2.12 eV. Therefore, the electrical conductivity of ZVO is improved by extracting zinc. The same analysis can be done for the ZVS, as the band gap decreases from 0.60 eV to 0 eV. Due to a much narrower bandgap, it is expected that ZVS exhibits better electrical conductivity than ZVO. The redox process can also be observed by analyzing the magnetic moment of vanadium as a function of zinc concentration (Tables S5 and S6 of the SI). At $x = 1$, $Zn_xV_2O_4$ and $Zn_xV_2S_4$ have only V^{3+} in their structure (magnetic moment $\approx 1.60\ \mu_B$). However, when zinc ions are extracted, V^{3+} ions are oxidized to V^{4+} (magnetic moment $\approx 0.9\ \mu_B$). For example, at $x = 1$, there are 16 V^{3+} ions in the $Zn_xV_2S_4$ and $Zn_xV_2S_4$ structures; at $x = 0.5$ there are 8 V^{3+} ions and 8 V^{4+} ions; and at $x = 0$, total oxidation of V occurs, i.e., only V^{4+} ions are observed. The vanadium magnetic moments and oxidation states of $Zn_xV_2O_4$ and $Zn_xV_2S_4$ for $x = 1$, $x = 0.5$, and $x = 0$ concentrations of zinc in the compound are shown in Tables S5 and S6 of the SI.

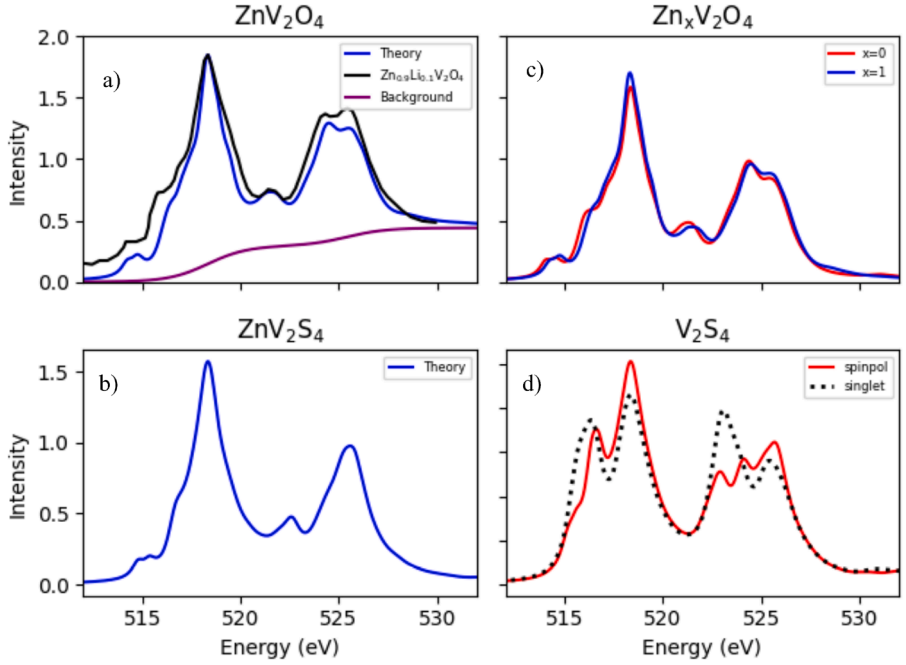

Fig. 4. Theoretical vanadium $L_{2,3}$-edge XANES spectra for $x = 1$ for a) ZVS and b) ZVO, compared to experimental results of $Zn_{0.9}Li_{0.1}V_2O_4$ [80]. Calculated vanadium $L_{2,3}$-edge XANES spectra at $x = 1$ and $x = 0$ zinc concentrations for c) ZVS and for d) the singlet and spin polarized state of zinc removed ZVS. Calculations performed using the RSPt code.

4. Discussion and conclusions

In this study, we have explored the intricate properties of ZnV_2O_4 (ZVO) and ZnV_2S_4 (ZVS) as potential cathode materials for zinc-ion batteries (ZIBs), along with the variant ZnV_2Se_4 (ZVSe), through density functional theory (DFT) calculations as well as theory of x-ray- and photoelectron spectroscopy that is based on multiplet ligand field theory. Our investigations provide a detailed mapping of their structural, electronic, magnetic, electrochemical, and spectroscopic (XPS and NEXAFS) properties, which are in close agreement with existing experimental data and offer predictive insights where such data are absent. The l-edge spectra are particularly interesting since a multi-configuration approach must be taken, due to the correlated nature of the valence electron states of the investigated systems, as well as the nature of the excitation process. Taking such an approach allows for excellent reproduction of known spectroscopic data for ZVO, and enables faith in the predicted values for ZVS.

Particularly, our findings highlight ZVS as a standout candidate for cathode applications in ZIBs due to its superior electrochemical performance compared to both synthesized and theoretically predicted cathodes. While ZVO shows promising electrochemical properties, challenges such as its wide band gap and poor capacity retention need to be addressed for it to be a viable cathode material. On the other hand, ZVSe, despite its poor electrochemical performance, may hold potential for other applications due to its unique properties.

Our work extends beyond the analysis of specific capacities and capacity retention, delving into changes in volume, electrical and ionic conductivity, thus providing a comprehensive understanding of the electrochemical behavior of these compounds. The theoretical insights gained from this study are well-aligned with available experimental data, paving the way for the development of high-performance cathode materials for ZIBs, with possible impact on sustainable energy solutions in the electrification of society.

CRediT authorship contribution statement

O.M. Sousa: Writing – review & editing, Writing – original draft, Validation, Software, Methodology, Investigation, Formal analysis, Conceptualization. **F. Sorgenfrei:** Writing – review & editing, Writing – original draft, Software, Methodology, Formal analysis. **F.O. Carvalho:** Validation, Methodology, Investigation, Formal analysis. **L.V.C. Assali:** Writing – review & editing, Validation, Methodology, Formal analysis, Conceptualization. **M.V. Lalic:** Writing – review & editing, Validation, Software, Methodology, Formal analysis. **P. Thunström:** Writing – review & editing, Validation, Methodology, Formal analysis. **C.Moyses Araujo:** Writing – review & editing, Validation, Methodology, Formal analysis. **O. Eriksson:** Writing – review & editing, Validation, Resources, Methodology, Funding acquisition, Formal analysis. **H.M. Petrilli:** Writing – review & editing, Supervision, Resources, Project administration, Formal analysis. **A.B. Klautau:** Writing – review & editing, Validation, Supervision, Resources, Project administration, Methodology, Funding acquisition, Formal analysis.

Declaration of competing interest

The authors Osmar Machado de Sousa, Felix Sorgenfrei, Felipe Oliveira Carvalho, Lucy Vitoria Credidio Assali, Milan Lalic, Patrik Thunström, Carlos Moyses Graca Araujo, Olle Eriksson, Helena Maria Petrilli and Angela Burlamaqui Klautau declare that they have no known competing financial interests or personal relationships that could have appeared to influence the work reported in this paper.

Acknowledgments

HMP, LVCA, ABK, and OMS acknowledge support from FAPESP (Project 2022/10095–8); ABK and OMS acknowledge FAPESPA; LVCA, HMP, ABK, MVL, FOC and OMS acknowledge support from CNPq and CAPES, Brazil. ABK acknowledges the INCT of Materials Informatics and the INCT of Spintronics and Advanced Magnetic Nanostructures. O.E. acknowledges support from the Wallenberg Initiative Materials Science (WISE) funded by the Knut and Alice Wallenberg Foundation as well as the Swedish Research Council (VR), the European Research Council (854843-FASTCORR), and eSSENCE. O.E. and CMA also acknowledge support from STandUP. The calculations were performed at the computational facilities of the CENAPAD-UNICAMP and CCAD-UFPA (Brazil) and facilities provided by NAISS, Sweden.

Supplementary materials

Supplementary material associated with this article can be found, in the online version, at doi:10.1016/j.actamat.2024.120468.

References

[1] K. Cai, S. Luo, J. Feng, J. Wang, Y. Zhan, Q. Wang, Y. Zhang, X. Liu, Recent advances on spinel zinc manganate cathode materials for zinc-ion batteries, Chem. Rec. (2022) 22, https://doi.org/10.1002/tcr.202100169.
[2] H. Wu, J. Hao, Y. Jiang, Y. Jiao, J. Liu, X. Xu, K. Davey, C. Wang, S.Z. Qiao, Alkaline-based aqueous sodium-ion batteries for large-scale energy storage, Nat. Commun. 15 (2024) 575, https://doi.org/10.1038/s41467-024-44855-6.
[3] M. Mirzaeian, Q. Abbas, M.R.C. Hunt, A. Galeyeva, R. Raza, Na-ion batteries, in: encyclopedia of smart materials, Elsevier, 2022, pp. 135–147, https://doi.org/10.1016/B978-0-12-815732-9.00052-8.
[4] V. A, B. John, T.D. M, Potassium-ion batteries: key to future large-scale energy storage? ACS Appl. Energy Mater. 3 (2020) 9478–9492, https://doi.org/10.1021/acsaem.0c01574.
[5] L. Deng, J. Qu, X. Niu, J. Liu, J. Zhang, Y. Hong, M. Feng, J. Wang, M. Hu, L. Zeng, Q. Zhang, L. Guo, Y. Zhu, Defect-free potassium manganese hexacyanoferrate cathode material for high-performance potassium-ion batteries, Nat. Commun. 12 (2021) 2167, https://doi.org/10.1038/s41467-021-22499-0.
[6] J. Bae, H. Park, X. Guo, X. Zhang, J.H. Warner, G. Yu, High-performance magnesium metal batteries *via* switching the passivation film into a solid electrolyte interphase, Energy Environ. Sci. 14 (2021) 4391–4399, https://doi.org/10.1039/D1EE00614B.
[7] C. Drosos, C. Jia, S. Mathew, R.G. Palgrave, B. Moss, A. Kafizas, D. Vernardou, Aerosol-assisted chemical vapor deposition of V_2O_5 cathodes with high rate capabilities for magnesium-ion batteries, J. Power Sources 384 (2018) 355–359, https://doi.org/10.1016/j.jpowsour.2018.02.074.
[8] Z.L. Xu, J. Park, J. Wang, H. Moon, G. Yoon, J. Lim, Y.J. Ko, S.P. Cho, S.Y. Lee, K. Kang, A new high-voltage calcium intercalation host for ultra-stable and high-power calcium rechargeable batteries, Nat. Commun. 12 (2021) 3369, https://doi.org/10.1038/s41467-021-23703-x.
[9] M. Wang, C. Jiang, S. Zhang, X. Song, Y. Tang, H.M. Cheng, Reversible calcium alloying enables a practical room-temperature rechargeable calcium-ion battery with a high discharge voltage, Nat. Chem. 10 (2018) 667–672, https://doi.org/10.1038/s41557-018-0045-4.
[10] G. Zampardi, F.L. Mantia, Open challenges and good experimental practices in the research field of aqueous Zn-ion batteries, Nat. Commun. 13 (2022) 687, https://doi.org/10.1038/s41467-022-28381-x.
[11] H. Tian, G. Feng, Q. Wang, Z. Li, W. Zhang, M. Lucero, Z. Feng, Z.L. Wang, Y. Zhang, C. Zhen, M. Gu, X. Shan, Y. Yang, Three-dimensional Zn-based alloys for dendrite-free aqueous Zn battery in dual-cation electrolytes, Nat. Commun. 13 (2022) 7922, https://doi.org/10.1038/s41467-022-35618-2.
[12] K. Zhang, K.O. Kirlikovali, J.M. Suh, J.W. Choi, H.W. Jang, R.S. Varma, O.K. Farha, M. Shokouhimehr, Recent advances in rechargeable aluminum-ion batteries and considerations for their future progress, ACS Appl. Energy Mater. 3 (2020) 6019–6035, https://doi.org/10.1021/acsaem.0c00957.
[13] G.A. Elia, K.V. Kravchyk, M.V. Kovalenko, J. Chacón, A. Holland, R.G.A. Wills, An overview and prospective on Al and Al-ion battery technologies, J. Power Sources 481 (2021) 228870, https://doi.org/10.1016/j.jpowsour.2020.228870.
[14] L. Zhou, A.M. Yao, Y. Wu, Z. Hu, Y. Huang, Z. Hong, Machine learning assisted prediction of cathode materials for Zn-ion batteries, Adv. Theory Simul. 4 (2021), https://doi.org/10.1002/adts.202100196.
[15] G. Fang, J. Zhou, A. Pan, S. Liang, Recent advances in aqueous zinc-ion batteries, ACS Energy Lett 3 (2018) 2480–2501, https://doi.org/10.1021/acsenergylett.8b01426.
[16] Y. Shi, Y. Chen, L. Shi, K. Wang, B. Wang, L. Li, Y. Ma, Y. Li, Z. Sun, W. Ali, S. Ding, An overview and future perspectives of rechargeable zinc batteries, Small (2020) 16, https://doi.org/10.1002/smll.202000730.
[17] X. Zeng, J. Hao, Z. Wang, J. Mao, Z. Guo, Recent progress and perspectives on aqueous Zn-based rechargeable batteries with mild aqueous electrolytes, Energy Storage Mater 20 (2019) 410–437, https://doi.org/10.1016/j.ensm.2019.04.022.
[18] T. Zhang, Y. Tang, S. Guo, X. Cao, A. Pan, G. Fang, J. Zhou, S. Liang, Fundamentals and perspectives in developing zinc-ion battery electrolytes: a comprehensive review, Energy Environ. Sci. 13 (2020) 4625–4665, https://doi.org/10.1039/D0EE02620D.

[19] H. Li, L. Ma, C. Han, Z. Wang, Z. Liu, Z. Tang, C. Zhi, Advanced rechargeable zinc-based batteries: recent progress and future perspectives, Nano Energy 62 (2019) 550–587, https://doi.org/10.1016/j.nanoen.2019.05.059.

[20] C. Xu, B. Li, H. Du, F. Kang, Energetic zinc ion chemistry: the rechargeable zinc ion battery, Angew. Chem. 124 (2012) 957–959, https://doi.org/10.1002/ange.201106307.

[21] P. Luo, W. Tang, W. Cai, J. Yang, W. Zhang, C. Zuo, G. Liu, Y. Xiao, S. Dong, Charged-optimized ZnO/ZnV_2O_4 composite hollow microspheres robust zinc-ion storage capacity, J. Solid State Chem. 301 (2021) 122371, https://doi.org/10.1016/j.jssc.2021.122371.

[22] X.Z. Zhai, J. Qu, S.M. Hao, Y.Q. Jing, W. Chang, J. Wang, W. Li, Y. Abdelkrim, H. Yuan, Z.Z. Yu, Layered birnessite cathode with a displacement/intercalation mechanism for high-performance aqueous zinc-ion batteries, Nano-Micro Lett 12 (2020) 56, https://doi.org/10.1007/s40820-020-0397-3.

[23] T. Lv, Y. Peng, G. Zhang, S. Jiang, Z. Yang, S. Yang, H. Pang, How about vanadium-based compounds as cathode materials for aqueous zinc ion batteries? Adv. Sci. 10 (2023) https://doi.org/10.1002/advs.202206907.

[24] C. Xu, Z. Yang, X. Zhang, M. Xia, H. Yan, J. Li, H. Yu, L. Zhang, J. Shu, Correction to: prussian blue analogues in aqueous batteries and desalination batteries, Nano-Micro Lett 13 (2021) 187, https://doi.org/10.1007/s40820-021-00715-2.

[25] K. Hurlbutt, S. Wheeler, I. Capone, M. Pasta, Prussian blue analogs as battery materials, Joule 2 (2018) 1950–1960, https://doi.org/10.1016/j.joule.2018.07.017.

[26] Y. Zhang, E.H. Ang, K.N. Dinh, K. Rui, H. Lin, J. Zhu, Q. Yan, Recent advances in vanadium-based cathode materials for rechargeable zinc ion batteries, Mater. Chem. Front. 5 (2021) 744–762, https://doi.org/10.1039/D0QM00577K.

[27] P. He, Q. Chen, M. Yan, X. Xu, L. Zhou, L. Mai, C.W. Nan, Building better zinc-ion batteries: a materials perspective, EnergyChem 1 (2019) 100022, https://doi.org/10.1016/j.enchem.2019.100022.

[28] C. Liu, Z. Neale, J. Zheng, X. Jia, J. Huang, M. Yan, M. Tian, M. Wang, J. Yang, G. Cao, Expanded hydrated vanadate for high-performance aqueous zinc-ion batteries, Energy Environ. Sci. 12 (2019) 2273–2285, https://doi.org/10.1039/C9EE00956F.

[29] F. Zhang, M.S. Whittingham, Hydrothermal synthesis and electrochemistry of a δ-type manganese vanadium oxide, Electrochem. Commun. 2 (2000) 69–71, https://doi.org/10.1016/S1388-2481(99)00143-5.

[30] M. Narayanasamy, B. Balan, C. Yan, S. Angaiah, Cauliflower-like nanostructured ZnV_2S_4 as a potential cathode material to boost-up high capacity and durability of the aqueous zinc-ion battery, Chin. Chem. Lett. 34 (2023) 108076, https://doi.org/10.1016/j.cclet.2022.108076.

[31] Y. Liu, C. Li, J. Xu, M. Ou, C. Fang, S. Sun, Y. Qiu, J. Peng, G. Lu, Q. Li, J. Han, Y. Huang, Electroactivation-induced spinel ZnV_2O_4 as a high-performance cathode material for aqueous zinc-ion battery, Nano Energy 67 (2020) 104211, https://doi.org/10.1016/j.nanoen.2019.104211.

[32] J. Wu, Q. Kuang, K. Zhang, J. Feng, C. Huang, J. Li, Q. Fan, Y. Dong, Y. Zhao, Spinel $Zn_3V_3O_8$: a high-capacity zinc supplied cathode for aqueous Zn-ion batteries, Energy Storage Mater 41 (2021) 297–309, https://doi.org/10.1016/j.ensm.2021.06.006.

[33] W. Tang, B. Lan, C. Tang, Q. An, L. Chen, W. Zhang, C. Zuo, S. Dong, P. Luo, Urchin-like spinel MgV_2O_4 as a cathode material for aqueous zinc-ion batteries, ACS Sustain. Chem. Eng. 8 (2020) 3681–3688, https://doi.org/10.1021/acssuschemeng.9b06613.

[34] C. Zuo, W. Tang, B. Lan, F. Xiong, H. Tang, S. Dong, W. Zhang, C. Tang, J. Li, Y. Ruan, S. Xi, Q. An, P. Luo, Unexpected discovery of magnesium-vanadium spinel oxide containing extractable Mg^{2+} as a high-capacity cathode material for magnesium ion batteries, Chem. Eng. J. 405 (2021) 127005, https://doi.org/10.1016/j.cej.2020.127005.

[35] N. Zhang, F. Cheng, Y. Liu, Q. Zhao, K. Lei, C. Chen, X. Liu, J. Chen, Cation-deficient spinel $ZnMn_2O_4$ cathode in $Zn(CF_3SO_3)_2$ electrolyte for rechargeable aqueous zn-ion battery, J. Am. Chem. Soc. 138 (2016) 12894–12901, https://doi.org/10.1021/jacs.6b05958.

[36] H. Zhang, J. Wang, Q. Liu, W. He, Z. Lai, X. Zhang, M. Yu, Y. Tong, X. Lu, Extracting oxygen anions from $ZnMn_2O_4$: robust cathode for flexible all-solid-state Zn-ion batteries, Energy Storage Mater 21 (2019) 154–161, https://doi.org/10.1016/j.ensm.2018.12.019.

[37] S. Islam, M.H. Alfaruqi, D.Y. Putro, S. Park, S. Kim, S. Lee, M.S. Ahmed, V. Mathew, Y. Sun, J. Hwang, J. Kim, In situ oriented Mn deficient $ZnMn_2O_4$@C nanoarchitecture for durable rechargeable aqueous zinc-ion batteries, Adv. Sci. 8 (2021), https://doi.org/10.1002/advs.202002636.

[38] Y. Yang, T. Shao, Y. Zhang, Y. Lu, M. Li, H. Liu, Q. Xu, Y. Xia, Anionic S-doping of a $ZnMn_2O_4$/CNTs cathode material enhances its Zn^{2+} storage performance in aqueous zinc-ion batteries, J. Power Sources 564 (2023) 232863, https://doi.org/10.1016/j.jpowsour.2023.232863.

[39] T. Shao, Y. Zhang, T. Cao, Y. Yang, Z. Li, H. Liu, Y. Wang, Yongyao Xia, Structural regulation of $ZnMn_2O_4$ cathode material by K, Fe-double doping to improve its rate and cycling stability for rechargeable aqueous zinc-based batteries, Chem. Eng. J. 431 (2022) 133735, https://doi.org/10.1016/j.cej.2021.133735.

[40] J. Luo, X. Liu, A. Yang, Z. Xie, First-principles calculation of ferromagnetic elements (Fe, Co)-doped ZnV_2O_4, SSRN Electron. J. (2022), https://doi.org/10.2139/ssrn.4136290.

[41] X. Liu, J. Luo, A. Yang, First-principles calculation of rare earth elements (Eu, Yb)-doped ZnV_2O_4, Ferroelectr 597 (2022) 119–129, https://doi.org/10.1080/00150193.2022.2092008.

[42] T.I. Al-Muhimeed, G.M. Mustafa, A.A. AlObaid, A. Mera, K. Shahzadi, M.M. AL-Anazy, Q. Mahmood, Role of trivalent substitution at octahedral side on ferromagnetism and transport properties of ZnX_2S_4 (X = Ti, V, Cr) spinels, Eur. Phys. J. Plus 137 (2022) 299, https://doi.org/10.1140/epjp/s13360-022-02389-0.

[43] M. Al-Qhtani, G. Mustafa, N. Mazhar, S. Bouzgarrou, Q. Mahmood, A. Mera, Z. Zaki, N. Mostafa, S. Alotaibi, M. Amin, Half metallic ferromagnetism and transport properties of zinc chalcogenides ZnX_2Se_4 (X = Ti, V, Cr) for spintronic applications, Mater 15 (2021) 55, https://doi.org/10.3390/ma15010055.

[44] D.J. Singh, L. Nordstron, Planewaves, Pseudopotentials and the LAPW Method, Springer, New York, 2006 second ed.

[45] P. Blaha, K. Schwarz, G.K.H. Madsen, D. Kvasnicka, J. Luitz, An augmented plane waves + local orbital program for calculating crystal properties, Karlheinz Schwarz, Techn. Universitat Wien, 2001, pp. 1–223.

[46] P. Hohenberg, W. Kohn, Inhomogeneous electron gas, Phys. Rev. 136 (1964) B864–B871, https://doi.org/10.1103/PhysRev.136.B864.

[47] W. Kohn, L.J. Sham, Self-consistent equations including exchange and correlation effects, Phys. Rev. 140 (1965) A1133–A1138, https://doi.org/10.1103/PhysRev.140.A1133.

[48] H.J. Monkhorst, J.D. Pack, Special points for brillouin-zone integrations, Phys. Rev. B 13 (1976) 5188–5192, https://doi.org/10.1103/PhysRevB.13.5188.

[49] J.P. Perdew, K. Burke, M. Ernzerhof, Generalized gradient approximation made simple, Phys. Rev. Lett. 77 (1996) 3865–3868, https://doi.org/10.1103/PhysRevLett.77.3865.

[50] V.I. Anisimov, J. Zaanen, O.K. Andersen, Band theory and Mott insulators: hubbard U instead of Stoner I, Phys. Rev. B 44 (1991) 943–954, https://doi.org/10.1103/PhysRevB.44.943.

[51] A.I. Liechtenstein, V.I. Anisimov, J. Zaanen, Density-functional theory and strong interactions: orbital ordering in mott-hubbard insulators, Phys. Rev. B 52 (1995) R5467–R5470, https://doi.org/10.1103/PhysRevB.52.R5467.

[52] G.K.H. Madsen, P. Novák, Charge order in magnetite. An LDA+ *U* study, Europhys. Lett. (EPL) 69 (2005) 777–783, https://doi.org/10.1209/epl/i2004-10416-x.

[53] V.I. Anisimov, O. Gunnarsson, Density-functional calculation of effective Coulomb interactions in metals, Phys. Rev. B 43 (1991) 7570–7574, https://doi.org/10.1103/PhysRevB.43.7570.

[54] V. Shrivastava, R. Nagarajan, Modulating the optical and magnetic properties of geometrically frustrated ZnV_2O_4 by the introduction of indium (nonmagnetic ions), iron, and chromium (magnetic ions), Dalton Trans 49 (2020) 15810–15820, https://doi.org/10.1039/D0DT02554B.

[55] H. Du, Q. Ma, X. Gao, T.S. Zhao, Cu/ZnV_2O_4 Heterojunction interface promoted methanol and ethanol generation from CO_2 and H_2O under UV–vis light irradiation, ACS Omega 7 (2022) 7278–7286, https://doi.org/10.1021/acsomega.1c07108.

[56] F. Tran, P. Blaha, Accurate band gaps of semiconductors and insulators with a semilocal exchange-correlation potential, Phys. Rev. Lett. 102 (2009) 226401, https://doi.org/10.1103/PhysRevLett.102.226401.

[57] O.M. Sousa, R.S. Araujo, S.M. Freitas, Calculation of the electronic and optical properties of $LiFe_5O_8$: an ab initio study, Comput. Theor. Chem. 1159 (2019) 27–30, https://doi.org/10.1016/j.comptc.2019.05.008.

[58] O.M. Sousa, A.F. Lima, M.V. Lalic, New insights into the electronic and optical properties of the $Bi_4M_3O_{12}$ (M = Si or Ge) scintillators, Opt. Mater. (Amst) 73 (2017) 642–646, https://doi.org/10.1016/j.optmat.2017.09.021.

[59] O.M. de Sousa, Study of the structural, electronic, and optical properties of the host matrices of $LiAl_5O_8$ and $LiGa_5O_8$ via DFT, Comput. Theor. Chem. 1123 (2018) 96–101, https://doi.org/10.1016/j.comptc.2017.11.015.

[60] T.M. Oliveira, A.F. Lima, M.G. Brik, S.O. Souza, M.V. Lalic, Electronic structure and optical properties of magnesium tetraborate: an ab initio study, Comput. Mater. Sci. 124 (2016) 1–7, https://doi.org/10.1016/j.commatsci.2016.07.007.

[61] C. Santos, A.F. Lima, M.V. Lalic, Electronic structure and optical properties of lithium tetraborate detector calculated using semi-local exchange correlation potential, Comput. Mater. Sci. 95 (2014) 271–275, https://doi.org/10.1016/j.commatsci.2014.07.038.

[62] A.S. Milošević, M.V. Lalić, Z.S. Popović, F.R. Vukajlović, An ab initio study of electronic structure and optical properties of multiferroic perovskites $PbVO_3$ and $BiCoO_3$, Opt. Mater. (Amst) 35 (2013) 1765–1771, https://doi.org/10.1016/j.optmat.2013.04.033.

[63] D. Koller, F. Tran, P. Blaha, Improving the modified Becke-Johnson exchange potential, Phys. Rev. B 85 (2012) 155109, https://doi.org/10.1103/PhysRevB.85.155109.

[64] S.J. Clark, M.D. Segall, C.J. Pickard, P.J. Hasnip, M.I.J. Probert, K. Refson, M. C. Payne, First principles methods using CASTEP, Z. Kristallogr. Cryst. Mater. 220 (2005) 567–570, https://doi.org/10.1524/zkri.220.5.567.65075.

[65] C.J. Pickard, On-the-fly pseudopotential generation in CASTEP, 2006.

[66] N. Govind, M. Petersen, G. Fitzgerald, D. King-Smith, J. Andzelm, A generalized synchronous transit method for transition state location, Comput. Mater. Sci. 28 (2003) 250–258, https://doi.org/10.1016/S0927-0256(03)00111-3.

[67] J.M. Wills, O. Eriksson, P. Andersson, A. Delin, O. Grechnyev, M. Alouani, Full-potential electronic structure method, Springer Berlin Heidelberg, Berlin, Heidelberg, 2010, https://doi.org/10.1007/978-3-642-15144-6.

[68] RSPt, Relativistic spin polarized toolkit, http://fplmto-rspt.org/, 2017.

[69] A. Grechnev, I. Di Marco, M.I. Katsnelson, A.I. Lichtenstein, J. Wills, O. Eriksson, Theory of bulk and surface quasiparticle spectra for Fe, Co, and Ni, Phys. Rev. B 76 (2007) 035107, https://doi.org/10.1103/PhysRevB.76.035107.

[70] P. Thunström, I. Di Marco, O. Eriksson, Electronic entanglement in late transition metal oxides, Phys. Rev. Lett 109 (2012) 186401, https://doi.org/10.1103/PhysRevLett.109.186401.

[71] J. Lüder, J. Schött, B. Brena, M.W. Haverkort, P. Thunström, O. Eriksson, B. Sanyal, I. Di Marco, Y.O. Kvashnin, Theory of *L*-edge spectroscopy of strongly correlated

systems, Phys. Rev. B 96 (2017) 245131, https://doi.org/10.1103/PhysRevB.96.245131.
[72] F. Sorgenfrei, M. Alouani, J. Schött, H.J.M. Jönsson, O. Eriksson, P. Thunström, Theory of x-ray absorption spectroscopy for ferrites, Phys. Rev. B 109 (2024) 115126, https://doi.org/10.1103/PhysRevB.109.115126.
[73] https://github.com/JohanSchott/impurityModel.
[74] M. Reehuis, A. Krimmel, N. Buttgen, A. Loidl, A. Prokofiev, Crystallographic and magnetic structure of ZnV_2O_4, Eur. Phys. J. B. 35 (2003) 311–316, https://doi.org/10.1140/epjb/e2003-00282-4.
[75] J. Cai, Z. Wang, S. Wu, Y. Han, J. Li, A Machine learning shortcut for screening the spinel structures of Mg/Zn ion battery cathodes with a high conductivity and rapid ion kinetics, Energy Storage Mater 42 (2021) 277–285, https://doi.org/10.1016/j.ensm.2021.07.042.
[76] O.M. Sousa, L.V.C. Assali, M.V. Lalic, C.M. Araujo, O. Eriksson, H.M. Petrilli, A. B. Klautau, Charging behavior of $ZnMn_2O_4$ and $LiMn_2O_4$ in a zinc- and lithium-ion battery: an ab initio study, J. Phys. Energy 6 (2024) 025025, https://doi.org/10.1088/2515-7655/ad39dc.
[77] N. Nitta, F. Wu, J.T. Lee, G. Yushin, Li-ion battery materials: present and future, Mater. Today 18 (2015) 252–264, https://doi.org/10.1016/J.MATTOD.2014.10.040.
[78] I.V.B. Maggay, L.M.Z. De Juan, M.T. Nguyen, T. Yonezawa, B.K. Chang, T.S. Chan, W.R. Liu, ZnV_2O_4: a potential anode material for sodium-ion batteries, J. Taiwan Inst. Chem. Eng. 88 (2018) 161–168, https://doi.org/10.1016/j.jtice.2018.03.052.
[79] M. Singha, R. Gupta, Transport properties of ZnV_2O_4 and its correlation to the doping at the cationic sites, J. Phys. 33 (2021) 375701, https://doi.org/10.1088/1361-648X/ac101d.
[80] M. Abbate, The O 1s and V 2p X-ray absorption spectra of vanadium oxides, 1994.
[81] C. Schmitz-Antoniak, N.V. Izarova, N. Svechkina, A. Smekhova, M. Stuckart, D. Schmitz, P. Kögerler, Polyoxopalladates as prototype molecular hydrogen uptake systems and novel in situ hydrogen detectors on the nanoscale, Eur. J. Inorg. Chem. 2019 (2019) 448–455, https://doi.org/10.1002/ejic.201800972.